

Article ID: 1007-4627(2016)02-0160-07

## Proton and Two-proton Emissions from Proton-rich Nuclei with $10 \leq Z \leq 20$

LIN Chengjian(林承键)<sup>1</sup>, XU Xinxing(徐新星)<sup>1</sup>, WANG Jiansong(王建松)<sup>2</sup>, SUN Lijie(孙立杰)<sup>1</sup>,  
JIA Huiming(贾会明)<sup>1</sup>, YANG Lei(杨磊)<sup>1</sup>, MA Peng(马朋)<sup>2</sup>, MA Junbing(马军兵)<sup>2</sup>,  
YANG Yanyun(杨彦云)<sup>2</sup>, JIN Shilun(金仕纶)<sup>2</sup>, HUANG Meirong(黄美容)<sup>2</sup>,  
BAI Zheng(白真)<sup>2</sup>, WU Zhendong(吴振东)<sup>1</sup>, YANG Feng(杨峰)<sup>1</sup>,  
HU Zhenguo(胡正国)<sup>2</sup>, WANG Meng(王猛)<sup>2</sup>, LEI Xiangguo(雷相国)<sup>2</sup>,  
ZHANG Huanqiao(张焕乔)<sup>1</sup>, XU Hushan(徐瑚珊)<sup>2</sup>, XIAO Guoqing(肖国青)<sup>2</sup>

(1. China Institute of Atomic Energy, Beijing 102413, China;

2. Institute of Modern Physics, Chinese Academy of Sciences, Lanzhou 730000, China)

**Abstract:** Proton (p) and two-proton (2p) emissions from the proton-rich nuclei with  $10 \leq Z \leq 20$  have been explored by the in-flight decay and implantation decay methods, respectively, in a series of experiments at the HIRFL-RIBLL facility. The in-flight 2p emissions from the excited states of  $^{28,29}\text{S}/^{26,27}\text{P}$  and  $^{17,18}\text{Ne}$  were studied by complete-kinematics measurements. Mechanisms of 2p decay and related p-p correlations have been explored. Obvious 2p correlated emissions have been observed in the cases of  $^{28,29}\text{S}$  but not in  $^{27,28}\text{P}$ , indicating the 2p halo plays an important role in the diproton emission. In the  $^{17,18}\text{Ne}$  cases, a small 2p opening angles were deduced by the HBT analyses, implying the BCS-BEC crossover may occur in the dilute nuclear matter. Moreover,  $^{27}\text{S}/^{26}\text{P}/^{25}\text{Si}$ ,  $^{22}\text{Si}/^{20}\text{Mg}$ ,  $^{23}\text{Si}/^{22}\text{Al}/^{21}\text{Mg}$ ,  $^{24}\text{Si}/^{23}\text{Al}$ , and  $^{36,37}\text{Ca}$  were implanted in a thin double-sided-silicon-strip detector and their  $\beta$ -delayed p and 2p decays have been measured by a surrounding silicon detector array under the continuous-beam mode. Important information on the nuclear spectroscopy, such as energy, lifetime, branching-ratio, and so on, has been extracted, which helps us to understand the nuclear structures of proton-rich exotic nuclei close to the drip-line.

**Key words:** proton emission; two-proton emission; proton-proton correlation; complete-kinematics measurement; implantation decay; proton-rich exotic nucleus

**CLC number:** O571.6      **Document code:** A      **DOI:** 10.11804/NuclPhysRev.33.02.160

### 1 Introduction

The historic discovery of the radioactivity opens a door to the subject of nuclear physics. Since the radioactivity was discovered by Henri Becquerel in 1896, several types of nuclear decay, such as  $\alpha$ ,  $\beta$ ,  $\gamma$  decays, fission, proton radioactivity, *etc.*, have been observed with the development of nuclear science. The newest one, two-proton (2p) radioactivity proposed by Goldanskii<sup>[1]</sup> more than half century ago, was discovered in  $^{45}\text{Fe}$ <sup>[2-3]</sup>,  $^{54}\text{Zn}$ <sup>[4]</sup>, and most likely  $^{48}\text{Ni}$ <sup>[5]</sup>. Nowadays, it becomes one of the most exciting topics in the field of radioactive-ion-beam physics<sup>[6-7]</sup>.

An unusual diproton (sometimes referred to  $^2\text{He}$ ) decay has been reported<sup>[8-10]</sup> through the investigation of correlations between two protons (p-p correlations), although the mechanism is still unclear. Thanks to the pairing effect, 2p may constitute a quasi-bound  $^1\text{S}$  state in the nuclear matter, especially amid the surrounding of low density matter like halo state. In this case, the valence 2p is spatially decoupled from the tightly-bound core; meanwhile the interaction between the two protons becomes important. It was suggested<sup>[6]</sup> that 2p halo would lead to a much larger spectroscopic factor for a direct 2p decay than for a sequential decay. Through the 2p events measured in

**Received date:** 18 Dec. 2015;      **Revised date:** 23 Apr. 2016

**Foundation item:** National Basic Research Program of China (973 Program)(2013CB834404); National Natural Science Foundation of China (10735100, 10727505, 11005156, U1432246, U1432127)

**Biography:** LIN Chengjian (1970-), male, Fuzhou, Fujian, Professor, working on the field of nuclear reactions and related nuclear structures; E-mail address: cjlin@ciae.ac.cn.

an experiment, we may learn their decay mechanism and further probe the p-p correlations.

When going away from the valley of stability,  $\beta$ -delayed particle emissions will be taken place due to the high decay energy and low binding energy of nucleon. Further, when approaching to the drip-line, direct particle emissions are energetically allowed. The study of exotic nuclei far from the stability line has been one of the frontiers of nuclear physics during the past few decades. A larger number of experimental and theoretical studies have been conducted to investigate the properties of exotic nuclei on both proton-rich and neutron-rich sides, which substantially broadens the scope of nuclear physics research<sup>[6–7,11–12]</sup>.

From 2004 to now, we have performed a series of experiments to study 2p emission from the proton-rich nuclei close to the drip line by using the HIRFL-RIBLL facility<sup>[13]</sup>. Early, in the  $^{29}\text{S}+^{28}\text{Si}$  experiment, an abnormally large total reaction cross section has been detected<sup>[14]</sup>, indicating the possibility of 2p halo/skin structure in  $^{29}\text{S}$ . Moreover, signatures of 2p emission were observed in the  $^{29}\text{S}+^{12}\text{C}$  reaction<sup>[15]</sup>. Later, starting from 2007, we focus on in-flight 2p emission from the excited states of  $^{17,18}\text{Ne}$  and  $^{28,29}\text{S}/^{27,28}\text{P}$  by means of the complete-kinematics measurements. The decay modes of 2p emissions from the excited states as well as the links to the initial configurations of their ground states have been explored. Meanwhile, starting from 2011, many proton-rich nuclei, such as  $^{27}\text{S}/^{26}\text{P}/^{25}\text{Si}$ ,  $^{22}\text{Si}/^{20}\text{Mg}$ ,  $^{23}\text{Si}/^{22}\text{Al}/^{21}\text{Mg}$ ,  $^{24}\text{Si}/^{23}\text{Al}$ , and  $^{36,37}\text{Ca}$  have been produced and implanted in a thin double-sided silicon strip detector (DSSD). The  $\beta$ -delayed p and 2p decays have been measured by a surrounding silicon detector array under the continuous-beam mode. Important information on the nuclear spectroscopy, such as energy, lifetime, branching-ratio, *etc.*, has been extracted. In this paper, we would like to review the recent researches, which are helpful to us

for understanding the diproton decay, p-p correlation, and the related nuclear structure of proton-rich exotic nuclei close to the drip-line.

## 2 In-flight decays

The in-flight decays, *i.e.* directly 2p emissions from the excited states of  $^{17,18}\text{Ne}$  and  $^{28,29}\text{S}/^{27,28}\text{P}$  have been explored by means of the complete-kinematics measurement. Details of the experimental procedure, results and discussions are described below.

### 2.1 Experimental procedure

The experiments were done at the Institute of Modern Physics, Lanzhou, China. The secondary radioactive beams were produced by the primary beams of  $^{20}\text{Ne}$  and  $^{32}\text{S}$ , respectively, with typical current of 100 enA, bombarding on the  $1589 \mu\text{m}$   $^9\text{Be}$  target, transported and purified through the RIBLL facility<sup>[13]</sup> by means of the combined  $B\rho$ - $\Delta E$ - $B\rho$  method, where  $^{27}\text{Al}$  degraders with different thicknesses were chosen to get the suitable momentum dispersion. The excited states were populated by bombarding on a secondary  $^{197}\text{Au}$  target via the Coulomb excitation. Typical secondary beam intensities were 200 and 800 pps for  $^{17}\text{Ne}$  and  $^{18}\text{Ne}$  with purities of 10% and 40%, respectively, 30 and 200 pps for  $^{28}\text{S}$  and  $^{29}\text{S}$  with purities of 1% and 3%, respectively.

A detector array consisting of two parallel plane avalanche counts, three/four large area silicon detectors (SD), four single-sided silicon strip detectors (SSSDs), and a  $6 \times 6$  array of CsI crystals coupled to PIN photodiodes was employed to perform the complete-kinematics measurement. As an example, Fig. 1 shows the schematic plot of the detector array used in the  $^{28,29}\text{S}$  experiments. In this arrangement, the opening angle covered by the detectors array for two protons was  $\pm 13^\circ$ .

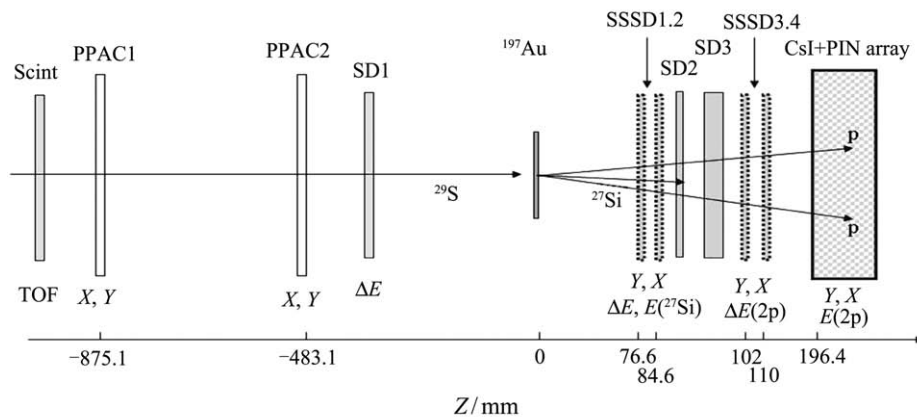


Fig. 1 A schematic plot of detector array for the complete-kinematics measurement.

The event-by-event analysis technique was employed in the selection of the true events produced by the  $N(Z, A) \rightarrow N(Z-2, A-2)+p+p$  processes. Firstly, parent nuclei  $N(Z, A)$ , *i.e.* the secondary beam particle, were selected on the two-dimensional particle identification (PID) spectrum of  $\Delta E$  versus ToF. Secondly, the PID of decay daughter nuclei  $N(Z-2, A-2)$ , *i.e.* the produce of heavy fragment, was achieved on the two-dimensional spectrum of  $\Delta E$  versus ER. Thirdly, the emitted light-particles like p, d, 2p,  $\alpha$ , were identified by the  $\Delta E$ -ER generated by the Si-CsI hodoscope. As an example, Fig. 2 shows the PID spectrums for  $^{28}\text{S}/^{27}\text{P}$  beams and their light-particle produces. The simultaneous 2p events can be clear selected by the

double-hits on the CsI array. For single-hit 2p events, *i.e.* two protons hit on the same CsI crystal, those events were simply omitted because their relative position cannot be resolved. It is shown that the 2p events locate within a band in which the energies of both  $\Delta E$  and Er are two times those of the 1p events. Fourthly, the cross-point-of-trajectories method was employed for trajectory tracking to reject the reactions did not take place in the target. In addition, a narrow time window ( $\sim 10$  ns) was applied to eliminate the contaminations of the daughter nuclei directly from the secondary beam as well as the accidental coincidences. Details of experimental procedure can be found in Ref. [9].

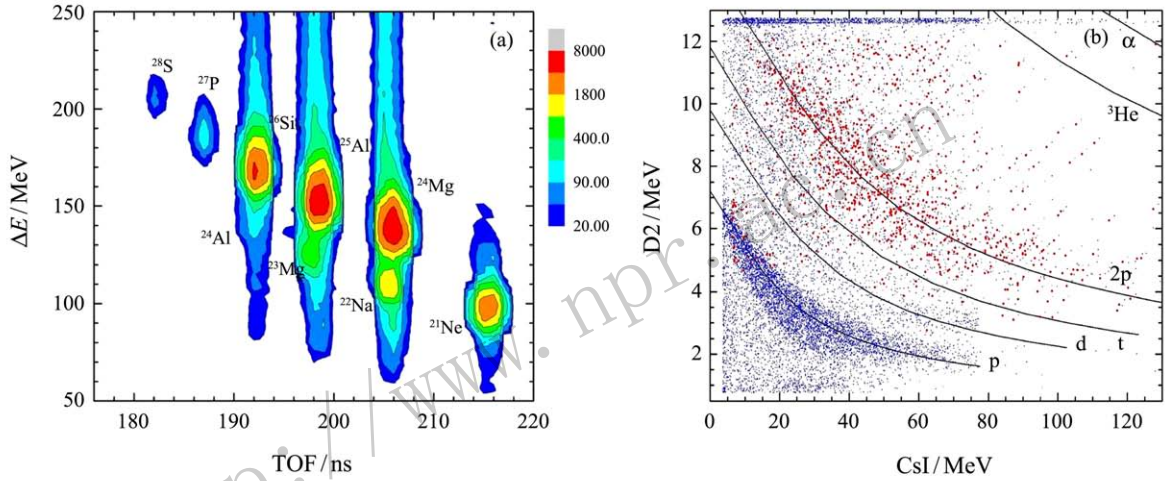


Fig. 2 (color online) PID spectrums of  $^{28}\text{S}/^{27}\text{P}$  beams (a) and light-particle products (b).

## 2.2 Kinematics reconstruction

After the pure events in the  $N(Z, A) \rightarrow N(Z-2, A-2)+p+p$  processes were selected, the invariant mass of final three-body system, the relative momentum ( $q_{pp} = |\mathbf{p}_1 - \mathbf{p}_2|/2$ ), the opening angle ( $\theta_{pp}^{c.m.}$ ), and the relative energy ( $E_{pp}$ ) of two protons can be deduced, on event-by-event basis, by the relativistic-kinematics reconstruction under the constraints of energy and momentum conservation.

In order to investigate the mechanisms of 2p decay, Monte Carlo (MC) simulations have been carried out. For the sake of simplicity, three schematic decay modes were employed to describe 2p emission, *i.e.*  $^2\text{He}$  decay, two-body sequential decay, and three-body phase-space simultaneous decay. In the first case, a preformed  $^2\text{He}$  resonance with the quasi-bound  $^1\text{S}$  configuration was assumed, leading to an enhanced peak at  $q_{pp}=20$  MeV/c<sup>[16]</sup> and small opening angle. In the latter two cases, no correlation between two protons was considered, resulting in an isotropic distribution

in opening angle. In the MC simulations, the energy and position resolutions of detectors, the experimental setup, and Coulomb deflections of heavy fragments in the target were taken into account.

Invariant-mass reconstructions of unbound 2p decaying states were performed via the total energy and the momentum of heavy fragments and two protons. With the assumption of decay to the ground state of the daughter nucleus, the invariant mass can be converted into the excitation energy according to mass excesses of ground states of parent and daughter nuclei. Fig. 3 shows the excitation-energy spectrums of  $^{28}\text{S}$  and  $^{27}\text{P}$  reconstructed by  $^{26}\text{Si}+p+p$  and  $^{25}\text{Al}+p+p$  events<sup>[17]</sup>, respectively. In the  $^{28}\text{S}$  spectrum, some resonant states are visible, say at  $\sim 6.0$  MeV and  $\sim 9.2$  MeV. In the  $^{27}\text{P}$  spectrum, the peak at 12.8 MeV (indicated by an arrow) is in good agreement with previous measurements of  $\beta$ -decayed 2p emission from  $^{27}\text{S}$ , which yielded values of 12.823 MeV<sup>[18]</sup> and 12.752 MeV<sup>[19]</sup> for the isobaric analogue state in  $^{27}\text{P}$ .

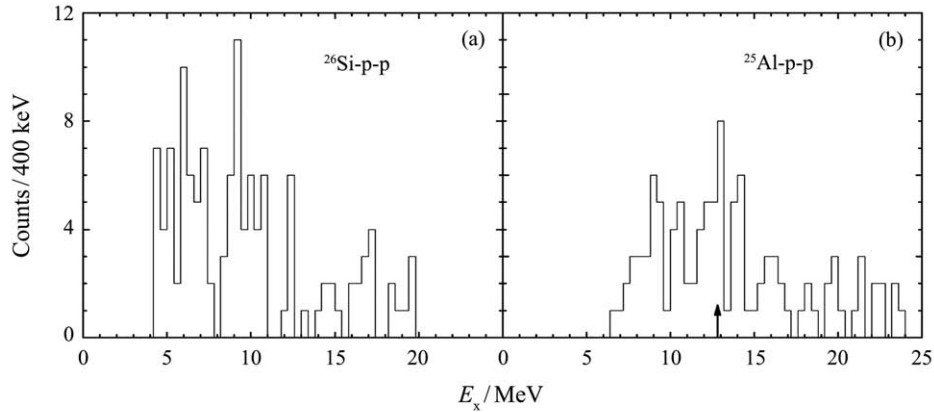


Fig. 3 Reconstructed excitation-energy spectra of  $^{28}\text{S}$  (a) and  $^{27}\text{P}$  (b).

### 2.3 Diproton decay and 2p halo— $^{28,29}\text{S}/^{27,28}\text{P}$

With the help of MC simulations, the mechanism of 2p decay can be understood by the relative momentum combined with opening angle of two protons. Fig. 4 shows the experimental results and MC simulated results of two protons emitted from excited levels in  $^{28}\text{S}$  and  $^{27}\text{P}$ <sup>[17]</sup>, respectively. The best fits (solid lines) were obtained by summing up the diproton emission (dashed lines) and the rest of three-body phase-space decay as well as two-body sequential decay with equal weight (dotted lines). Branch ratios of diproton

emission were determined as  $20_{-7}^{+6}\%$  and  $7 \pm 5\%$  with  $\chi^2_{\text{min}}/\text{pt} = 1.5$  and  $1.6$  for  $^{28}\text{S}$  and  $^{27}\text{P}$ , respectively, where errors were derived by the  $\chi^2$  analysis. In addition, fits by pure three-body decay (dash-dotted lines) were also performed to check up the effects of adding diproton branch, those yield  $\chi^2/\text{pt} = 2.5$  and  $1.9$  for  $^{28}\text{S}$  and  $^{27}\text{P}$ , respectively. For the  $^{28}\text{S}$  case, fits are obviously improved when diproton components are considered. While for the  $^{27}\text{P}$  case, fits show that three-body simultaneous decay and/or two-body sequential decay are dominant.

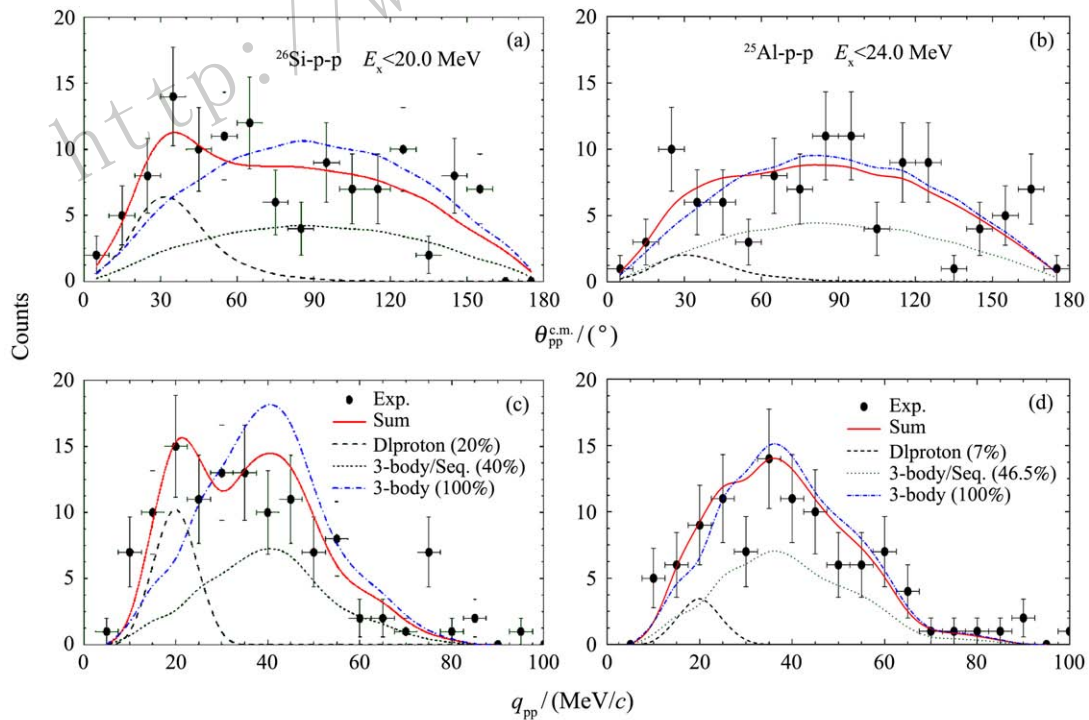


Fig. 4 (color online) Distributions of the opening angle (top) and the relative momentum (bottom) of two protons emitted from excited states less than 20.0 MeV in  $^{28}\text{S}$  (left) and 24.0 MeV in  $^{27}\text{P}$  (right), respectively. Solid lines show sums of the diproton emission (dashed lines) and the rest of 3-body phase-space decay and sequential two-body decay (dotted lines) with equal weight. Fits by pure 3-body decay (dash-dotted lines) are also plotted for comparison.

Besides, the  $^{29}\text{S}/^{28}\text{P}$  cases show the similar results as those of  $^{28}\text{S}/^{27}\text{P}$  cases mentioned above. In the  $^{29}\text{S}$  case, 2p events emitted from the 10.0 MeV excited state clearly exhibit a feature of diproton decay with a branching ratio of  $29_{-11}^{+10}\%$ <sup>[9]</sup>. However, no obvious signatures of diproton decay were found in the  $^{28}\text{P}$  case<sup>[20]</sup>.

Experimental distributions of 2p emissions from excited states in the even- $Z$  nucleus  $^{28,29}\text{S}$  are distinct from those in the odd- $Z$  nucleus  $^{27,28}\text{P}$ , implying their decay mechanisms are different. In the interpretation of large deformed orbits with large angular momentum existed in high-lying excited states, it was considered that strong anisotropy of the Coulomb barrier could result in a forward focusing in the angular distribution<sup>[21]</sup>. Deformed orbits are expected to exist in high-lying excited states of both  $^{28,29}\text{S}$  and  $^{27,28}\text{P}$ . However, only  $^{28,29}\text{S}$  show the forward focusing in 2p angular correlation while  $^{27,28}\text{P}$  show anisotropic angular distribution. It indicates that the deformation is not the cause of the anisotropy of 2p opening angle distribution. Obviously, the observed p-p correlations are relative to odd or even proton number, *i.e.* proton configuration in the initial state. In another explanation, correlated 2p direct emission maybe relevant to 2p skin/halo structure which possibly occur in a nucleus close to the proton drip-line due to the pairing interaction. There exists *s*-wave 2p halo in the ground states of  $^{28,29}\text{S}$  while *p*-wave 1p halo in  $^{27,28}\text{P}$ . It was suggested that<sup>[6]</sup> there should be such a halo effect in excited states as long as the two protons still significantly occupy low- $l$  orbits. In this case, the wave functions of 2p halo states in parent nuclei have a plenty overlap with those of 2p daughter states, which results in a much larger spectroscopic factor for direct 2p emission, such as the diproton decay. Different from this, the similar overlap with 2p daughter states is very small in the 1p halo nucleus. Therefore, the obvious anisotropy of the angular correlation of two protons was observed in the experimental measurement of the 2p halo nuclei  $^{28,29}\text{S}$ , but not in the 1p halo nuclei  $^{27,28}\text{P}$ . There exists a link between excited-state emission and ground state configuration.

#### 2.4 The BCS/BEC crossover— $^{17,18}\text{Ne}$

Hanbury-Brown Twiss (HBT) interferometry<sup>[22]</sup> has been widely employed to probe the space-time character of two-particle emitting source in subatomic physics. Recently, the HBT method was applied to the two-neutron halo nuclei like  $^6\text{He}$ ,  $^{11}\text{Li}$ , and  $^{14}\text{Be}$ <sup>[23]</sup> but not yet to the 2p halo nuclei nowadays. With high statistics of 2p emission events,  $^{17,18}\text{Ne}$  data allow us to do the HBT analyses. The momentum correlation

function is defined as  $C(\mathbf{q}) = N_2(\mathbf{q})/[N_1(\mathbf{p}_1)N_1(\mathbf{p}_2)]$ , where  $\mathbf{q}$  is the relative momentum of the proton pair,  $\mathbf{q} = |\mathbf{p}_1 - \mathbf{p}_2|/2$ .  $N_2$  is the relative momentum distribution of the proton pair measure in the experiment and  $N_1$  the momentum distribution of single proton reconstructed by the MC simulation.

The momentum correlation functions for 2p emitted from  $^{17,18}\text{Ne}$  nuclei are shown in Fig. 5. The inclusive data represent all the 2p events from  $^{17,18}\text{Ne}$ , which may include some sequential decay and some accidentally coincident events; while the exclusive data represent the events in  $^{17,18}\text{Ne} \rightarrow ^{15,16}\text{O} + \text{p} + \text{p}$  processes. Through the HBT analyses using a Gaussian shape as the source size, the p-p distances inside  $^{17,18}\text{Ne}$  nuclei are determined as  $5.17_{-0.08}^{+0.09}$  fm and  $5.44_{-0.17}^{+0.19}$  fm by the exclusive data, respectively.

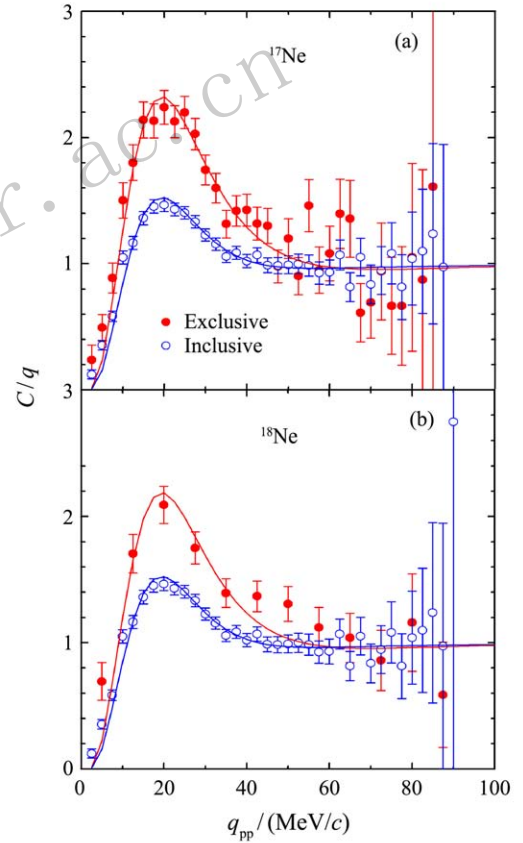


Fig. 5 (color online) Momentum correlation functions of 2p emitted from  $^{17,18}\text{Ne}$ .

Taking  $^{17}\text{Ne}$  as an example, the distance from 2p to their core was calculated as 3.4 fm by a three-body model<sup>[24]</sup>. Thus the opening angle between two protons was deduced as  $74.5^\circ$  by a simple trigonometric relation. This value is in good agreement with theoretical calculations<sup>[25–26]</sup>, indicating that BCS/BEC crossover<sup>[27]</sup> phenomenon may occur in the  $^{17}\text{Ne}$ , *i.e.* the surroundings of low density matter, as shown in



Fig. 6.

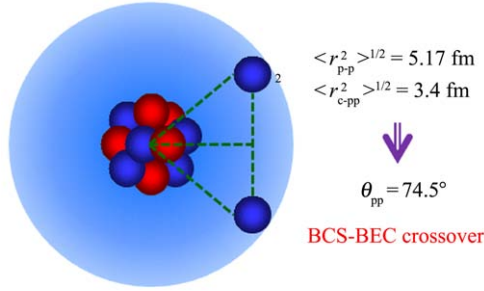


Fig. 6 (color online) The BCS/BEc crossover inside the  $^{17}\text{Ne}$  nucleus.

### 3 Implantation decays

The implantation decays, *i.e.* proton-rich nuclei  $^{27}\text{S}/^{26}\text{P}/^{25}\text{Si}$ ,  $^{22}\text{Si}/^{20}\text{Mg}$ ,  $^{23}\text{Si}/^{22}\text{Al}/^{21}\text{Mg}$ ,  $^{24}\text{Si}/^{23}\text{Al}$ , and  $^{36,37}\text{Ca}$  have been implanted in a thin DSSD. The  $\beta$ -delayed p/2p decays and possible direct p/2p decays have been measured by a surrounding silicon detector array under the continuous-beam mode. Details of the experimental procedure, results and discussions are described as following.

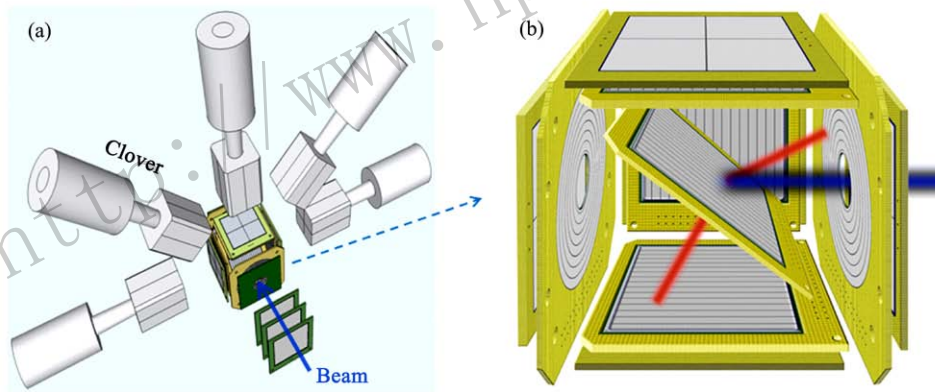


Fig. 7 (color online) A typical detector array used in the  $^{27}\text{S}$  experiment for detecting  $\beta$ -delayed p/2p emissions(a), and details of the center silicon cube. The front detectors are removed to see the inner structure(b).

Under the continuous-beam mode, the decays were measured and correlated to the preceding implantations by using position and time information. The system allows us to measure protons with energies down to about 200 keV without obvious  $\beta$  pileup in the energy spectrum.

### 3.2 Experimental results

Massive amounts of data have been recorded, and data analyses are still in progress. Some experimental results are published<sup>[28–29]</sup>. Here, we briefly show the preliminary results of the  $^{27}\text{S}$  experiment. Fig. 8 plots the PID spectrum of  $^{27}\text{S}/^{26}\text{P}/^{25}\text{Si}$  beams. The inten-

### 3.1 Experimental procedure

The secondary beams of  $^{27}\text{S}/^{26}\text{P}/^{25}\text{Si}$ ,  $^{22,23,24}\text{Si}/^{22,23}\text{Al}/^{20,21}\text{Mg}$ , and  $^{36,37}\text{Ca}$  were produced by the primary beams of  $^{32}\text{S}$ ,  $^{28}\text{Si}$  and  $^{40}\text{Ca}$ , respectively, bombarding on the  $^9\text{Be}$  target, purified and transported through the RIBLL facility, and finally implanted into a thin DSSD. Decayed  $\beta$ -particles and charged-particles, like p, 2p, were detected by a surrounding detector array.

Fig. 7 shows a typical detector array used in the  $^{27}\text{S}$  experiment, with the capability of detecting 2p emissions. The whole detector array is illustrated in Fig. 7(a), which contains a center silicon cube, surrounding by 5 clover-type HPGe detectors for  $\gamma$ -rays detection, and 3 quadrant silicon detectors (QSDs) installed upstream as  $\Delta E$  detectors. The structure of the center silicon cube is demonstrated in Fig. 7(b). A 60  $\mu\text{m}$  DSSD with dip angle of  $45^\circ$  locates at the center as the register of implanted nuclei. The charged particles decayed from the implanted nuclei are measured by the DSSD-QSD combined detectors on every side. The detecting efficiency for 1p and 2p events are 66% and 20%, respectively, estimated by a MC simulation.

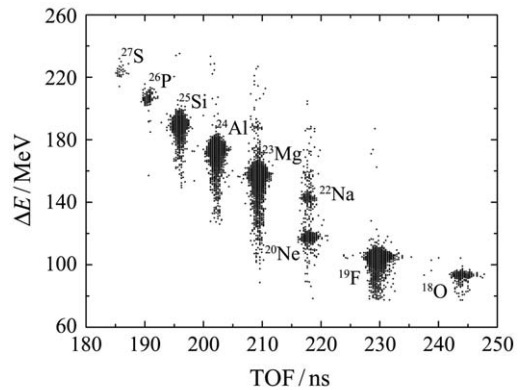


Fig. 8 PID spectrum of  $^{27}\text{S}/^{26}\text{P}/^{25}\text{Si}$  beams.

sity of  $^{27}\text{S}$  and  $^{26}\text{P}$  are 1 pps and 5 pps with purities of 0.1% and 0.5%, respectively. The energy spectrum of  $\beta\text{p}$  and  $\beta 2\text{p}$  decay from  $^{27}\text{S}$  is shown in Fig. 9. Some resonant states above the proton emission threshold are clearly identified, and all the excited states below 3 MeV are observed for the first time in this measurement.

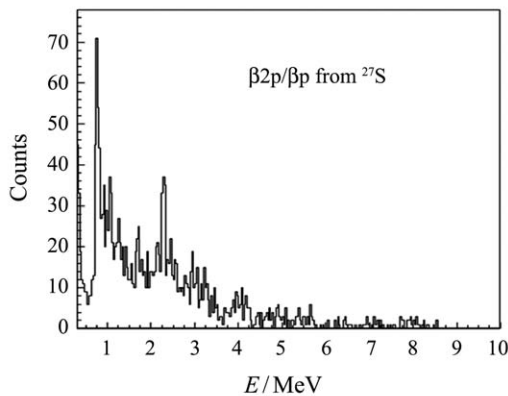


Fig. 9 Energy spectrum of  $\beta\text{p}$  and  $\beta 2\text{p}$  decay from  $^{27}\text{S}$ .

## 4 Summary and outlook

In summary, a series of experiments have been performed to study the direct as well as  $\beta$ -delayed  $\text{p}/2\text{p}$  decays from proton-rich nuclei with  $10 \leq Z \leq 20$ . The main conclusions are

- $2\text{p}$  correlated emissions were observed in  $^{28,29}\text{S}$  but not in  $^{27,28}\text{P}$ , indicating the diproton emission is enhanced by the  $2\text{p}$  halo;
- HBT analyses show  $2\text{p}$  in  $^{17,18}\text{Ne}$  have small opening angles, showing a signature of BCS-BEC crossover in the dilute nuclear matter;
- $\beta\text{p}/\beta 2\text{p}$  decays of  $^{27}\text{S}/^{26}\text{P}/^{25}\text{Si}$ ,  $^{22}\text{Si}/^{20}\text{Mg}$ ,  $^{23}\text{Si}/^{22}\text{Al}/^{21}\text{Mg}$ ,  $^{24}\text{Si}/^{23}\text{Al}$ , and  $^{36,37}\text{Ca}$  have been studied, which is helpful to understand the nuclear structures of proton-rich exotic nuclei close to the drip-line.

In the future, the link between diproton emission and  $2\text{p}$  halo is desired to be explored further, which requires a precise theoretical description embedded in the MC simulation. Besides, more  $\text{p}/2\text{p}$  and  $\beta\text{p}/\beta 2\text{p}$  emitters are planned to be investigated.

### References:

- [1] GOLDANSKI V I. Nucl Phys, 1960, **19**: 482.
- [2] GIOVINAZZO J, BLANK B, CHARTIER M, *et al.* Phys Rev Lett, 2002, **89**: 102501.
- [3] PFUTZNER M, BADURA E, BINGHAM C, *et al.* Eur Phys J A, 2002, **14**: 279.
- [4] BLANK B, BEY A, CANCEL G, *et al.* Phys Rev Lett, 2005, **94**: 232501.
- [5] DOSSAT C, BEY A, BLANK B, *et al.* Phys Rev C, 2005, **72**: 054315.
- [6] BLANK B, PLOSZAJCZAK M. Rep Prog Phys, 2008, **71**: 046301.
- [7] PFÜTZNER M, KARNY M, GRIGORENKO L V, *et al.* Rev Mod Phys, 2012, **84**: 567.
- [8] RACITI G, CARDELLA G, DE Napoli M, *et al.* Phys Rev Lett, 2008, **100**: 192503.
- [9] LIN C J, XU X X, JIA H M, *et al.* Phys Rev C, 2009, **80**: 014310.
- [10] CHARITY R J, WISER T D, MERCURIO K, *et al.* Phys Rev C, 2009, **80**: 024306.
- [11] BERGE M J G. Phys Scr T, 2013, **152**: 014013
- [12] BLANK B, BERGE M J G. Prog Part Nucl Phys, 2008, **60**: 403
- [13] SUN Z Y, ZHAN W L, GUO Z Y, *et al.* Nucl Instr Meth A, 2003, **503**: 496.
- [14] LIU Z H, RUAN M, ZHAO Y L, *et al.* Chin Phys Lett, 2004, **21**: 1711.
- [15] LIN C J, XU X X, ZHANG G L, *et al.* AIP Conf Proc, 2007, **961**: 117.
- [16] KOONIN S E. Phys Lett B, 1977, **70**: 43.
- [17] XU X X, LIN C J, JIA H M, *et al.* Phys Lett B, 2013, **727**: 126.
- [18] BORREL V, JACMART J C, POUGHEON F, *et al.* Nucl Phys A, 1991, **531**: 353.
- [19] CANCEL G, ACHOURI L, ÄYSTÖ J, *et al.* Eur Phys J A, 2001, **12**: 377.
- [20] XU X X, LIN C J, JIA H M, *et al.* Phys Rev C, 2010, **81**: 054317.
- [21] MUKHA I, ROECK E, BATIST L, *et al.* Nature, 2006, **439**: 298.
- [22] HANBURY-BROWN R, TWISS R Q. Nature, 1956, **178**: 1046.
- [23] MARQUES F M, *et al.* Phys Lett B, 2000, **476**: 219; Phys Rev C, 2001, **64**: 061301R.
- [24] GARRIDO E, FEDOROV D V, JENSEN A S. Nucl Phys A, 2004, **733**: 85.
- [25] OISHI T, HAGINO K, SAGAWA H. Phys Rev C, 2010, **82**: 024315.
- [26] BERTULANI C A, HUSSEIN M S. Phys Rev C, 2007, **76**: 051602R.
- [27] HAGINO K, SAGAWA H, CARBONELL J, *et al.* Phys Rev Lett, 2007, **99**: 022506.
- [28] SUN L J, LIN C J, XU X X, *et al.* Chin Phys Lett, 2015, **32**: 012301.
- [29] SUN L J, XU X X, LIN C J, *et al.* Nucl Instr Meth A, 2015, **804**: 1.